CrossMark

RESEARCH PAPER

N, S co-doped carbon dots with high quantum yield: tunable fluorescence in liquid/solid and extensible applications

Mei Yang · Xinlei Meng · Baoyan Li · Shusheng Ge · Yun Lu

Abstract A set of the highly fluorescent N, S co-doped carbon dots (NSCDs) were prepared through one-step hydrothermal synthesis at different temperature with citric acid as the carbon source and cysteamine as the N, S source. The NSCDs synthesized at 200 °C show significant quantum yield (81%) due to its optimal structure. The structure of the NSCDs changed with varying degrees of carbonization/aromatization and different content of multifunctional groups of C=O, $-NH_2$, $-OH$, $-SH$, and N, S-aromatic heterocycte under different preparation temperatures, thus exhibiting tunable fluorescence. Especially, the obtained NSCDs exhibited a blue fluorescence in solution state and changed from strong blue to yellowish-green in its solid state under UV light as a result of the increase in preparation temperature. The as-prepared NSCDs can be used in selective detection of complex anions such as $Cr_2O_7^{2-}$ and $Fe(CN)_6^{3-}$, cell imaging, and preparation of fluorescent composite films.

M. Yang · X. Meng · B. Li · S. Ge · Y. Lu (✉)
Department of Polymer Science and Engineering, State Key Laboratory of Coordination Chemistry, Collaborative Innovation Center of Chemistry for Life Sciences, Key Laboratory of High Performance Polymer Materials and Technology (Nanjing University), Ministry of Education, School of Chemistry and Chemical Engineering, Nanjing University, Nanjing 210046, People's Republic of China
e-mail: yunlu@nju.edu.cn

Introduction

The investigation of carbon materials with nanostructure is of great importance due to their unique properties and promising application in many areas. As a novel fluorescent nanomaterial, carbon dots (CDs) show superior characteristics such as outstanding water solubility, facile functionalization, low toxicity, favorable biocompatibility, high sensitivity and selectivity to target analytes and excellent photostability, and have promoted a great deal of interest in developing bioimaging, medical diagnose, chemical sensors, and photovoltaic devices (Baker and Baker 2010; Li et al. 2011, 2012; Shen et al. 2012).

In the several ways for preparing CDs, hydrothermal technology has become the most commonly used one because of its simple equipment without need for multistep and complex synthetic conditions, as well as modifying the CDs surface with different functional groups more easily. In this method, many precursors have been applied to produce CDs (Yang et al. 2011; Zhou et al. 2012; Mirtchev et al. 2012). In general, chemical doping with N or S element aiming to tune compositions and structures of CDs is considered very effective to intrinsically improve the properties of carbon materials. N-doping CDs (N-CDs) not only remain almost all the advantages

🖄 Springer

of blank CDs, but also efficiently enhance the photoluminescence (PL) quantum yield (QY) due to the similar size of nitrogen with carbon atom and the strong valence bonds between nitrogen and carbon atoms (Xu et al. 2015a, b; Lu et al. 2016; Hou et al. 2016). N-CDs synthesized with citric acid and ethylenediamine was a typical example, and its 80% QY and applications in sensors and bioimaging have been paid close attention (Zhu et al. 2013). S-doped CDs (S-CDs) showed a much improved photoluminescence properties compared with blank CDs mainly thanks to that sulfur atom could act as a catalytic center for redox reaction to introduce more passivated surface defects in CDs (Liang et al. 2012). S-CDs have been prepared by selecting suitable compounds such as sodium citrate and sodium thiosulfate etc. as precursors (Xu et al. 2015a, b). In addition, some N, S co-doped CDs (NSCDs) have been reported and showed novel properties (Ding et al. 2014; Samantara et al. 2015; Song et al. 2016). For instance, the NSCDs prepared by solid-phase thermal treatment of glutathione were used for highly selective and sensitive detection of Hg^{2+} (Wang et al. 2014a, b). The NSCDs prepared by using citric acid and L-cysteine as precursors were served as a fluorescence probe for highly sensitive detection of free chlorine (Xue et al. 2015). However, previous research mainly focused on the fluorescence and applications of CDs in aqueous solution, and solid-state photoluminescence of CDs have rarely been reported because of the fluorescence quenching in the aggregation state. Thus, it is still a challenge to prepare the fluorescent CDs with strong photoluminescence in both solution and the solid state, high QY, and stability against photobleaching.

In this paper, we chose a simple combination of citric acid with cysteamine to prepare NSCDs via a simple hydrothermal synthesis. The effect of hydrothermal temperature on fluorescence property of the as-prepared NSCDs in both solution and the solid state was investigated. Based on the detailed characterization, the structure and possible photo luminescence mechanism of the NSCDs were discussed. Besides, multifunctional applications of the as-prepared NSCDs such as selective detection of $Cr_2O_7^{2-}$ and $Fe(CN)_6^{3-}$, cell imaging and preparing fluorescent composite films have been demonstrated.

Experimental

Reagents and chemicals

Citric acid monohydrate was purchased from Chemical Reagent (Nanjing, China). Cysteamine was obtained from Adamas-beta (Shanghai, China). All other reagents used in this work are analytical grade and used as received without further purification. Doubly deionized water (18.2 MΩcm at 25 °C) prepared by a Milli-Q (MQ) water system was used throughout all experiments.

Synthesis of N, S co-doped CDs (NSCDs)

Citric acid monohydrate (0.21 g) and cysteamine (0.077 g) were mixed and dissolved in 20 mL deionized water. The mixture was then transferred into a polyphenyl autoclave (volume of 25 mL) and went through a hydrothermal treatment at different temperatures respectively (from 160 to 260 °C, 20 °C intervals) for 12 h. After cooling down to room temperature, the obtained solution was centrifuged (10,000 rpm) for 15 min to remove the precipitate. The obtained solution was concentrated at 80 °C, further isolated and purified by using silica gel chromatography with a mixture of methanol/ethyl acetate (3:1) as eluent and then made into the solid powders under freeze-drying.

Characterizations

The fluorescence spectral measurements were taken with HORIBA Jobin Yvon FluoroMax. UV-Vis absorption spectra were recorded by PerkinElmer Lambda 35. High-resolution transmission electron microscopy (HRTEM) observation was carried out with a JEM-2100F transmission electron microscope (JEOL, Japan) operated at an accelerating voltage of 200 kV. Fourier-transform infrared spectra (FTIR) of solid-state samples (KBr matrix) were recorded with a Bruker VECTOR22 spectrometer. The diameter and size distribution of the as-prepared NSCDs were evaluated by dynamic light scattering (DLS) using Brookhaven instrument (BI-200SM). The X-ray photoelectron spectra (XPS) were collected with a ESCALB MK-IIphotoelectron spectrometer. X-ray diffraction (XRD) analysis was carried out using X-ray powder diffractometer system (D8 AD-VANCE). Elemental analysis was performed on an Elementar Vario EL analyzer. ^1H NMR spectra were

obtained on a 400-Bru spectrometer 400 MHz and reported as parts per million (ppm) from the internal standard TMS using DMSO as the solvent. Mass spectrometry analyses were performed on the SHIMADZU LCMS-2020 Instrument.

Quantum yield measurements

The QY of the NSCDs was measured by comparing the integrated intensities and the UV absorbance value of NSCDs excited at 360 nm with quinine sulfate (QY = 0.54 in 0.1 M H_2SO_4) as the standard, and calculated according to the equation of $QYs = QY_R (F_s/A_s) (A_R/F_R) (n_s/n_R)^2$. Where the subscripts "$s$" and "$R$" refer to the sample of NSCDs and the reference quinine sulfate respectively, A is the absorbance value, F is the measured integrated emission intensity, and n is the refractive index.

Applications of the NSCDs

Experimental details for NSCDs applications, including the preparation of fluorescent composite films, sensitive detection for $Cr_2O_7^{2-}$ and $Fe(CN)_6^{3-}$, and fluorescent stains in cells imaging, are described in the supporting information.

Results and discussion

In the preparation process of NSCDs, the solutions obtained by premixing citric acid and cysteamine in deionized water were respectively heated at 160, 180, 200, 220, 240, and 260 °C for 12 h. After cooling down to room temperature, almost all solutions exhibited strong blue fluorescence under irradiation of 365 nm UV light, while under visible light excitation, emission varied from colorless to pale yellow, and finally deep yellow with the increase of preparation temperature (Fig. 1a). Also, the QY of the NSCDs prepared at different hydrothermal temperatures was measured which presented the non-linear change trend with the rising of the temperature. That is, their QY showed an increase from 76 to 81% for $NSCD_{160-200}$, and a decrease from 77 to 69% for $NSCD_{220-260}$ (Fig. S1 and Table S1). These experimental results suggested that the structure and property of NSCDs are temperature dependent, and thus understanding clearly the influence of preparation temperature on the structures of NSCDs is necessary. From FTIR spectra (Fig. 1b), it can be seen that all NSCDs samples possessed the abundant oxygen-containing groups such as O-H (3423 cm^{-1}), C-O (1215 cm^{-1}), and C=O (1730 cm^{-1}). This is due to the high temperature and sufficient oxygen environment provided by hydrothermal condition. The O-H vibration bands were broad for $NSCD_{160-200}$ but narrow for $NSCD_{220-260}$ and the stretching vibrations of C=O/ C-O became weaker from $NSCD_{160}$ to $NSCD_{260}$, manifesting that the degree of dehydration/carbonization of the NSCDs samples was enhanced with the increase of hydrothermal temperature. Stretching vibrations of C=C (1569 cm^{-1}), C-N = (1400 cm^{-1}), C=N (1640 cm^{-1}), and N-H (3200 cm^{-1}) bonds were observed, indicating the formation of polyaromatic structures with the doped
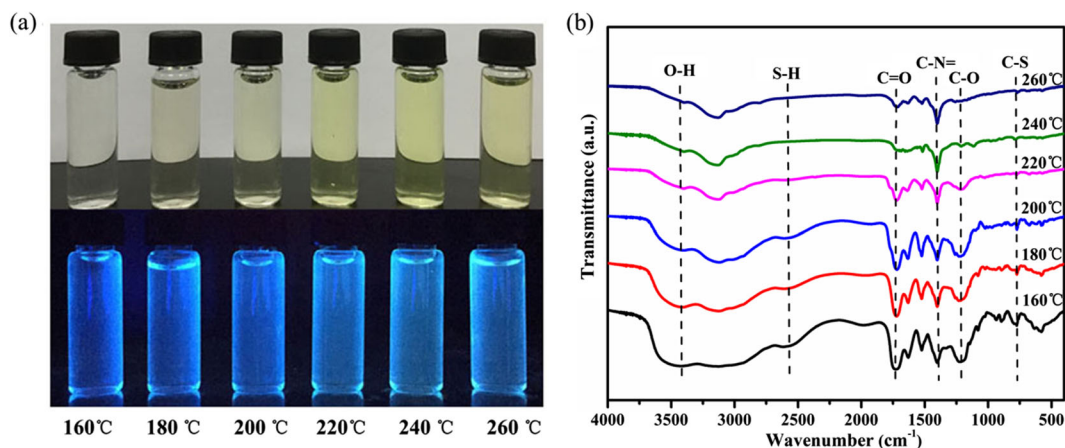

Fig. 1 a Photographs (*above*, under daylight and *below*, *under* 365 nm UV light) and b FTIR spectra of NSCDs prepared at different temperatures

N atoms in the NSCDs during the reaction process (Zhou et al. 2013; Wang et al. 2012). An enhancement of C-N=bond at 1400 cm^{-1} for the NSCD$_{160-260}$ implied the increase of polyaromatic structures with the increased hydrothermal temperature in the samples. Besides, the stretching vibration peak of S-H (2603 cm^{-1}) and −C-S- (near 780 cm^{-1}) became weaker for NSCD$_{160-220}$ and even difficult to be detected for NSCD$_{240-260}$, showing that the S atoms have also been doped into NSCDs framework, maybe forming other species of oxidation at elevated hydrothermal temperature.

As NSCD$_{200}$ showed the highest QY value among all NSCD samples, the further structural characterization was made on NSCD$_{200}$ and other two samples prepared respectively at the temperature lower or higher than 200 °C, that is, NSCD$_{160}$ and NSCD$_{260}$. ^{1}H NMR results (Fig. S2) provided the detail information of the CH of aromatic ring (7–9 ppm) and the CH of the functional groups (around 1, 3, and 4 ppm), implying the structure of NSCDs with a carbon core and some functional groups (Liu et al. 2007; Krysmann et al. 2012). And the peaks at ca.7.5 ppm for aromatic ring

hydrogen increased and at ca.12.5 for carboxyl hydrogen correspondingly decreased from NSCD$_{160}$, NSCD$_{200}$ to NSCD$_{260}$, revealing the expansion of the polyaromatic conjugated structures. The overall XPS spectra (Fig. S3) and the core region spectra of C 1s, N 1s, O 1s, and S 2p (Fig. 2) showed that carbon, nitrogen, oxygen, and sulfur were on the surface of the NSCD$_{160, 200, 260}$ and content of C=O in the NSCDs decreased corresponding to the increase in preparation temperature (Table S2), which is consistent with the FTIR results. The fitting results of C 1s in Fig. 2 showed that the peak attributed to sp^2 carbon atoms up-shifted to a higher binding energy (287.8 eV) for NSCD$_{260}$ comparing with that of NSCD$_{200}$ (284.5 eV) and NSCD$_{160}$ (283.6 eV), further demonstrating the expansion of conjugated structure. In addition, the fitting results of S 2p for NSCD$_{160}$ and NSCD$_{200}$ displayed two peaks at around 163 eV assigned to S 2p 2/3 and S 2p 1/3 of the C-S-C covalent bonds, respectively, due to their spin-orbit couplings (Ding et al. 2014; Dong et al. 2013), while for NSCD$_{260}$ there was an additional peak at 167.7 eV assigned to the oxidized sulfur species (−C–SO$_x$–C–, x = 2–4) such as sulfate or sulfonate (Yang
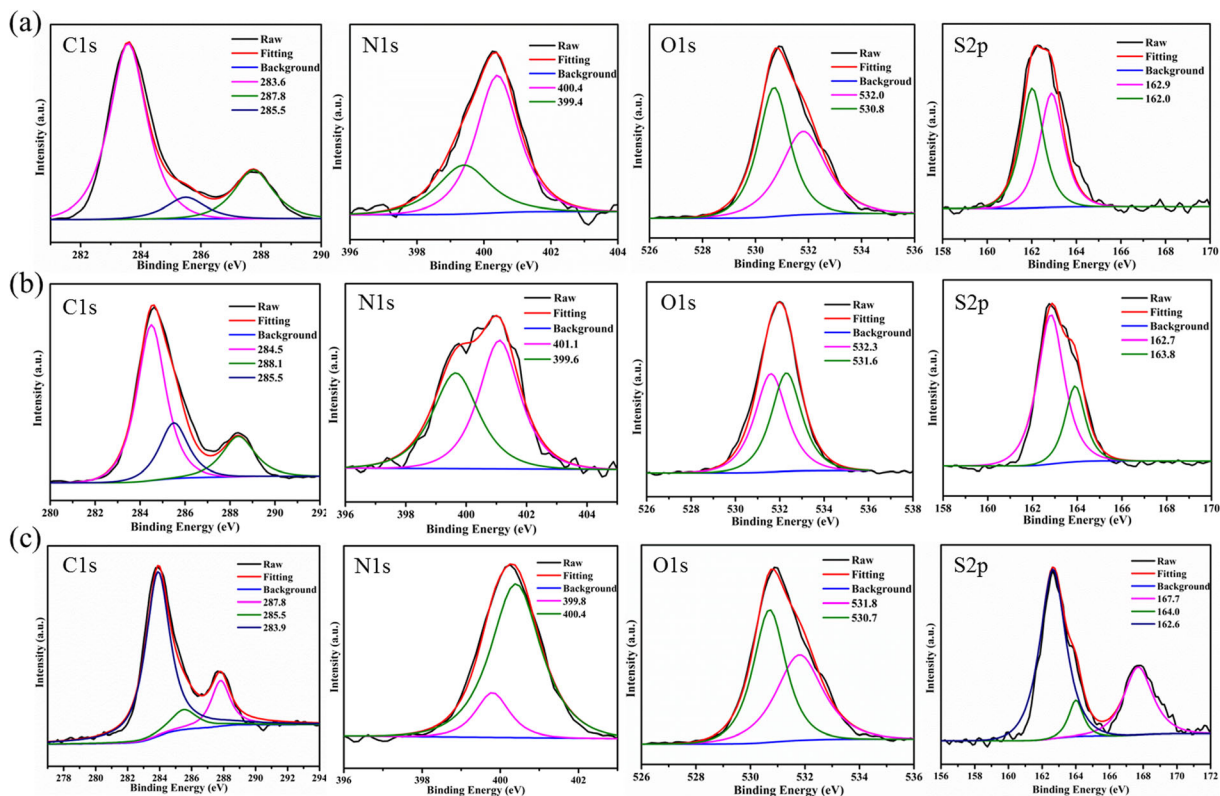

Fig. 2 XPS high-resolution survey scan of C 1s, N 1s, O 1s, and S 2p region of NSCD$_{160}$ (a), NSCD$_{200}$ (b) and NSCD$_{260}$ (c)
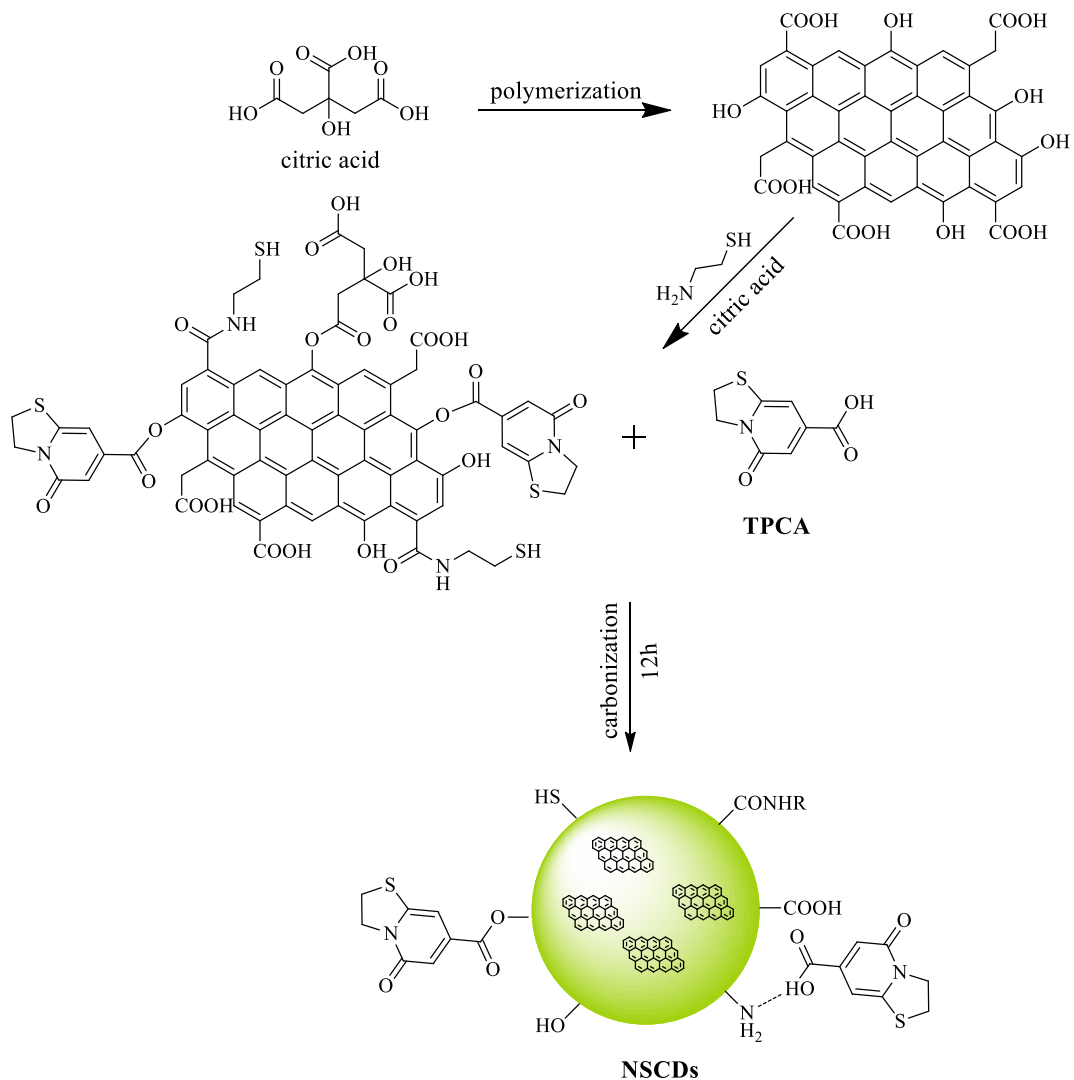
Fig. 3 The potential formation procedures of NSCDs

et al. 2012), which agrees with the phenomenon without S-H vibration peak in FTIR result of $NSCD_{260}$. The oxidized SOx species doped in the NSCDs are chemically inactive for redox reaction because they nearly have no any contribution toward fluorescence. This also explains well the fluorescence weakening for $NSCD_{260}$. Moreover, as shown in the results of elemental analysis (Table S3), compared with $NSCD_{160}$ and $NSCD_{200}$, $NSCD_{260}$ possesses less C and more O/N content confirming again the formation of SOx species and polyaromatic structures. ^{1}H NMR and XPS results indicated that, in our case, the optimized temperature for preparing the NSCDs with high fluorescence is 200 °C. The temperature increase is conducive to the continuous

generation of energy traps below 200 °C, thus contributes to the PL QY rising of samples; while the temperature above 200 °C could lead to the excessive carbonization and consequent decrease of QY values of NSCDs.

To clearly explain the possible photoluminescence mechanism of the NSCDs, we carried out the hydrothermal reaction of the single citric acid at the optimal temperature of 200 °C for 12 h, and the as-prepared product displayed its QY only 0.78%. This fully demonstrated that the participation of cysteamine was crucial, which contributed to the formation of doping N and S and multiple oxygen/nitrogen functional groups in the NSCDs under the reaction condition, and thus greatly

enhanced the fluorescence of NSCDs. By carefully separating and purificating the obtained NSCDs with silica gel chromatography, a fluorescent organic compound, 5-oxo-2,3-dihydro-5H-[1,3] thiazolo-[3,2-a] pyridine-7-carboxylic acid (TPCA, measured QY = 0.70) was isolated, and its molecular structure was proven by its FTIR (Fig. S4), ^{1}H NMR and MS spectra (Fig. S5) (Kasprzyk et al. 2015). The TPCA detected should be

related to the reaction system and reaction process. In our case, firstly, a small amount of citric acid was carbonized into graphene structure as carbon core by condensation polymerization (Dong et al. 2012). The carboxyl and hydroxyl groups hanged on the core surface reacted with cysteamine and residual citric acid to form a larger polyaromatic structure and the TPCA molecules. At the same time, the free TPCA molecules
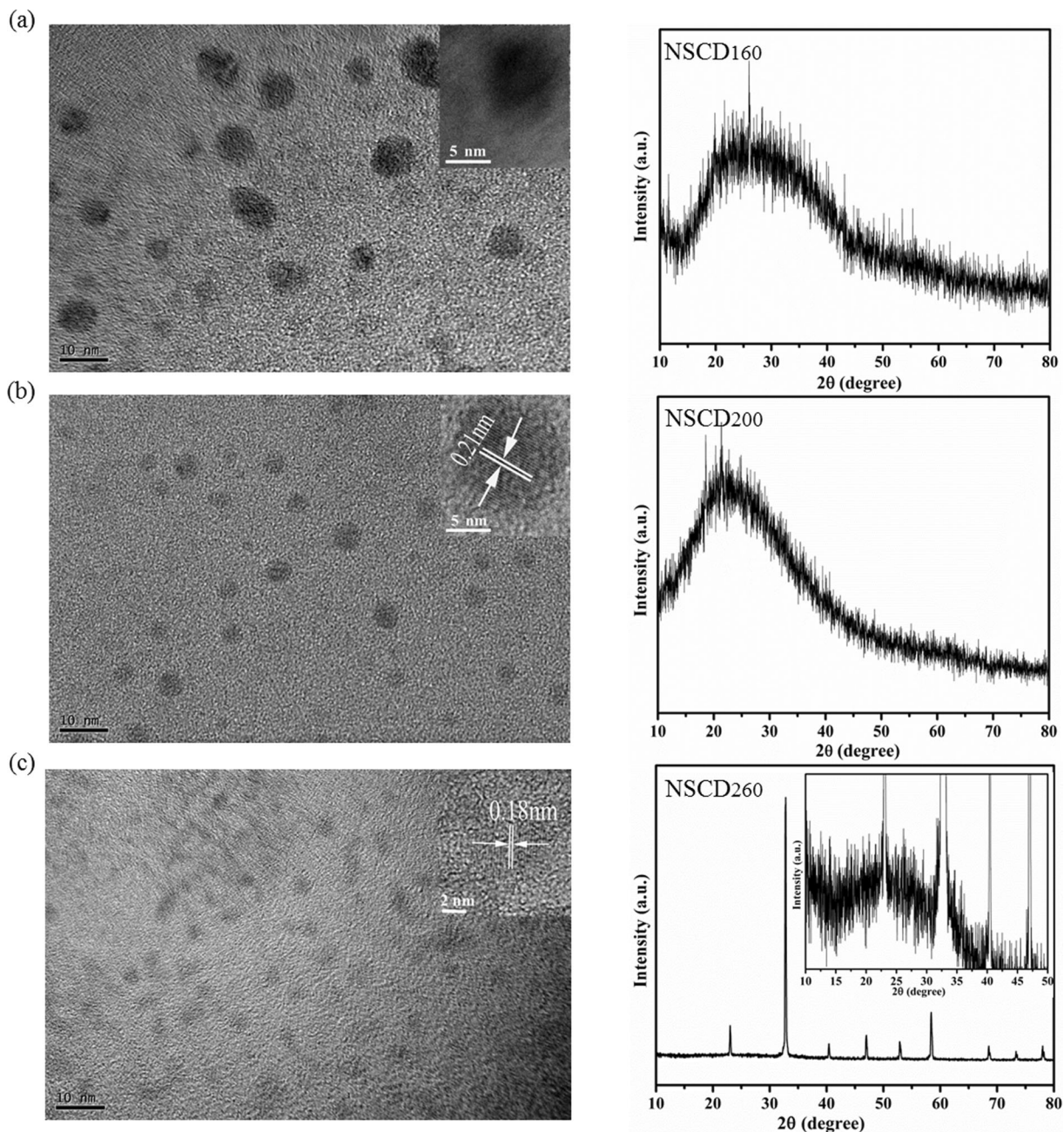

Fig. 4 HRTEM images (*left*) and XRD patterns (*right*) of $NSCD_{160}$ (**a**), $NSCD_{200}$ (**b**) and $NSCD_{260}$ (**c**)

could also be connected in/on to the polyaromatic structure through covalent or hydrogen bond during the reaction process which could be proved by different chemical shifts of TPCA and NSCDs (Figs. S2 and S5). Finally, the NSCDs with varying degrees of carbonization/aromatization and multifunctional groups of C=O, $-NH_2$, $-OH$, $-SH$, and N, S-aromatic heterocyte were formed under different hydrothermal temperature conditions. The possible formation mechanism of the NSCDs was shown in Fig. 3.

The formation process of NSCDs can be further explained through analyzing the HRTEM images and XRD graphs (Fig. 4). The HRTEM images showed that $NSCD_{160, 200, 260}$ presented a nearly spherical shape with uniform in size of around 7.8, 5.6, and 3.2 nm (Fig. S6), respectively, and a good dispersion. The difference of particle size for three samples was not obvious, indicating that the PL mechanism of NSCDs was due to the contributions of their surface states rather than the quantum size effects. Interestingly, the HRTEM images of NSCDs prepared at varied temperatures showed a different structural order degree (insets in Fig. 4, left). For instance, only $NSCD_{200}$ and $NSCD_{260}$ possessed crystalline structures with the interplanar lattice fringes of 0.21 and 0.18 nm, respectively, which can be assigned to (100) and (102) crystalline planes of graphite (Qu et al. 2013). Further, the XRD results of NSCDs have been proved to be well matched with the HRTEM ones. It can be noticed that, for $NSCD_{160}$ and $NSCD_{200}$, a wide peak at around 25° related to the graphene structure was observed and narrowing under elevated preparation temperature (Fig. 4a, b, right), meaning the different degree of crystallinity of samples.

While for $NSCD_{260}$, a XRD pattern of sulfates (For example, $(NH_4)_2SO_4$ and NH_4HSO_4) was presented, which maybe come from the interaction of the trace oxidized sulfur species generated at elevated hydrothermal temperature and the amino in the system. The XRD intensity of the sulfate with high crystallinity was so high that the diffraction peak of the graphene structure cannot be detected, which actually existed (inset of Fig. 4c, right).

In this work, the obtained NSCDs showed a unique luminescence, that is, the emission changed from excitation-independent to excitation-dependent as excitation wavelength varied from 300 to 400 nm and from 420 to 520 nm, respectively, which has been shown in Fig. 5a taking the $NSCD_{200}$ as a representative. The reasons were identified as the contribution of surface fluorophores such as C=O, $-NH_2$, $-OH$, $-SH$, and the N, S-aromatic heterocyte offered from TPCA for the former, and that of carbon core state for the latter (Krysmann et al. 2012; Bao et al. 2015). Besides this case, it can be seen that the fluorescence spectra of solution showed a continuous red shift followed by the increase of the concentration (Fig. 5b) mainly due to the stronger photo reabsorption with the enrichment of the solution (Zhang et al. 2014).

The sample of $NSCD_{200}$ highly diluted with the concentration of 10 μg mL^{-1} was selected to test its potential applications owing to its efficient fluorescence even in low concentration. Similar to the conventional CDs, $NSCD_{200}$ showed a sensitive responsiveness to solution pH, high PL stability toward ionic strength and good ability to resist photobleaching (Fig. S7), which met the most basic requirements for practical
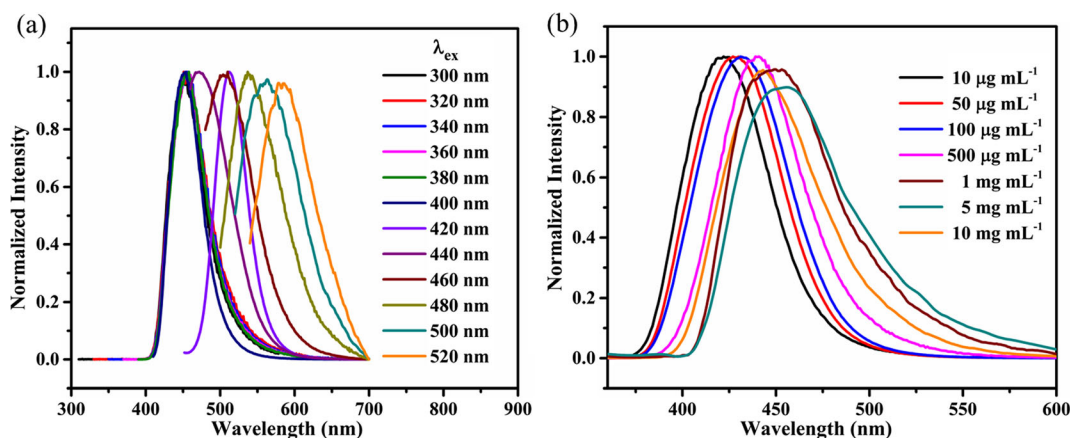

Fig. 5 Fluorescence emission spectra of $NSCD_{200}$ **a** measured at different excitation wavelengths in water (10 mg mL^{-1}) and **b** excited at 345 nm at different concentrations
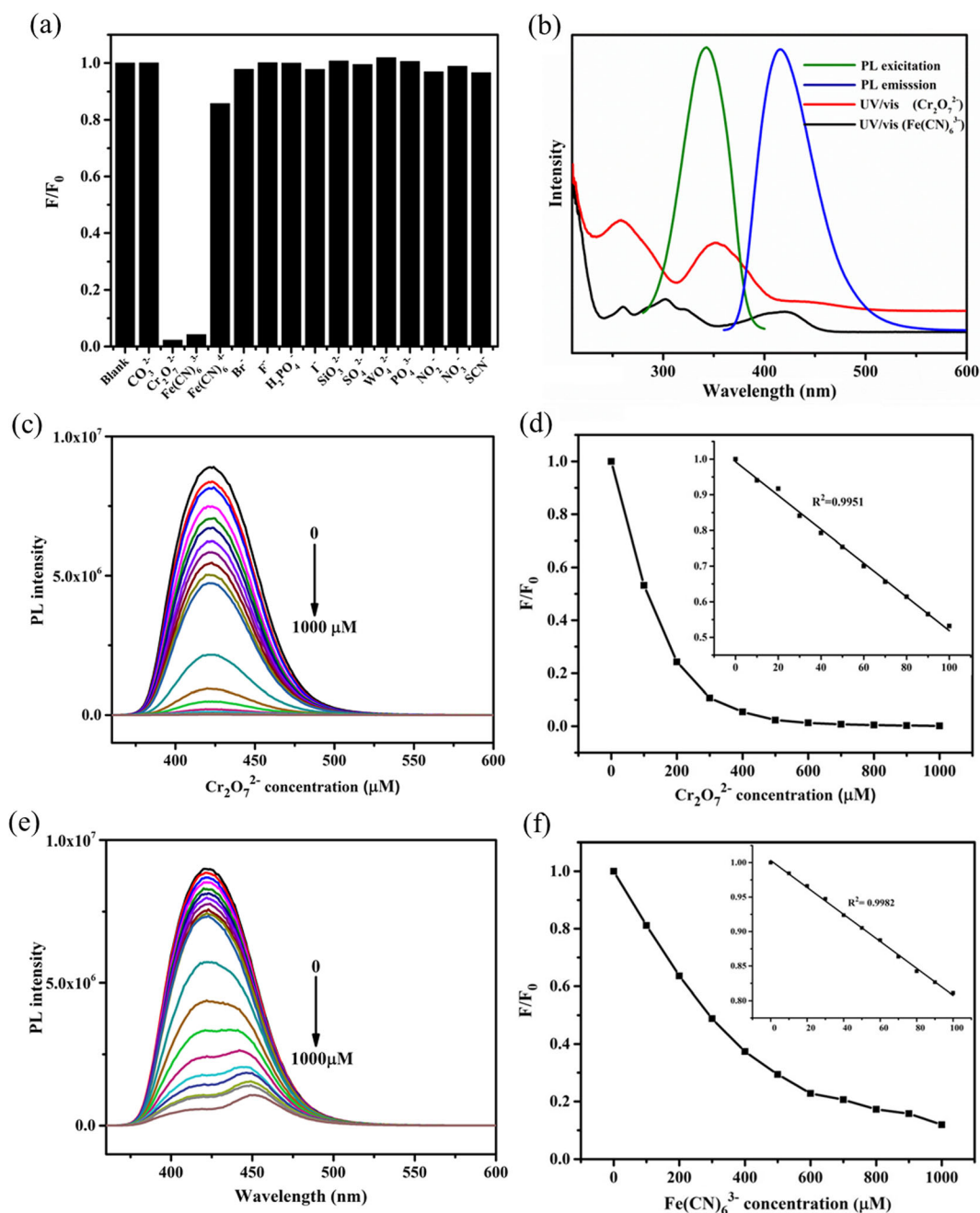
Fig. 6 a Relative fluorescence intensities (F/F_0) of the NSCD$_{200}$ solution after addition of 50 μM various anions. b Fluorescence excitation and emission spectra of NSCDs and UV−Vis absorption spectra of $Cr_2O_7^{2-}$ and $Fe(CN)_6^{3-}$. c, e Emission spectra of NSCD$_{200}$ solution measured with excitation of 345 nm in the presence of different concentrations of $Cr_2O_7^{2-}$ or $Fe(CN)_6^{3-}$ (0–1000 μM), respectively. d, f Fluorescence quenching degree F/F_0 of NSCD$_{200}$ as a function of $Cr_2O_7^{2-}$ and $Fe(CN)_6^{3-}$ concentration. *Insets* d, f are the magnification of the linear of the expression of F/F_0 against $Cr_2O_7^{2-}/Fe(CN)_6^{3-}$ concentration (0–100 μM), respectively

use. The NSCDs kept stable in acid, alkaline or salt solution, implying their good environment applicability. Different from the conventional CDs used to be single

metal ion sensor for detection of Fe^{3+}, Hg^{2+} etc., NSCD$_{200}$ exhibited a sensitive response in fluorescence intensity to complex anions such as $Cr_2O_7^{2-}$ and
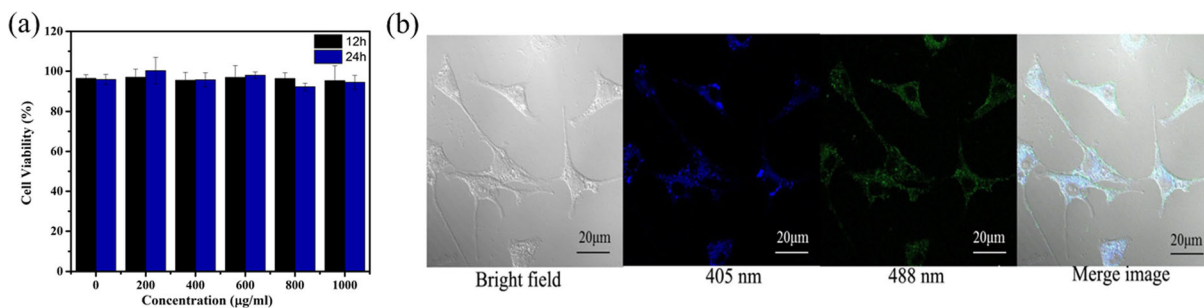
Fig. 7 a Viability of SH-SY5Y cells after incubation of 12/24 h with different concentrations of $NSCD_{200}$ by the MTT assay. **b** Confocal microscopy images of SH-SY5Y cells treated with $NSCD_{200}$ (100 µg mL^{-1})

$Fe(CN)_6^{3-}$ even with their very low concentration (50 µM) (Fig. 6a), which extended the species for the detection of ions. Also, the PL intensity almost kept unchanged in the presence of other anions under the same conditions, meaning that the $NSCD_{200}$ as a sensor is of a strong anti-interference capability. In the case of $Cr_2O_7^{2-}$, inner filter effect was considered to be responsible for the quenched fluorescence of $NSCD_{200}$, viz., the absorption bands of $Cr_2O_7^{2-}$ fully overlapped with the emission and excitation bands of $NSCD_{200}$ (Fig. 6b), facilitating the electron-exchange between Cr(VI) and the $NSCD_{200}$ and thus quenching the emitted light from the CDs (Zheng et al. 2013). For $Fe(CN)_6^{3-}$, besides the weaker inner filter effect, the main factor for fluorescence quenching of $NSCD_{200}$ may be attributed to the transfer of electrons from excited CDs to the Fe^{3+} ions in $Fe(CN)_6^{3-}$ coordinated to free hydroxyl or amino groups on the surface of $NSCD_{200}$ (Wu et al. 2009; Zhao et al. 2014). By contrast, for the detected $Fe(CN)_6^{4-}$, since such photoinduced electron transfer is infeasible due to the lower electron withdrawing ability of Fe^{2+} in $Fe(CN)_6^{4-}$ than Fe^{3+}, no fluorescence response to $NSCD_{200}$ was observed. The sensitivity

measurement results for $Cr_2O_7^{2-}$ and $Fe(CN)_6^{3-}$ indicated that with the increase of $Cr_2O_7^{2-}$ and $Fe(CN)_6^{3-}$ concentrations (0–1000 µM), the PL intensity decreased gradually (Fig. 6c–f). The calculated limits of detection to $Cr_2O_7^{2-}$ and $Fe(CN)_6^{3-}$ were 0.28 and 0.38 µM respectively, showing the advantage for detecting trace complex anions in industrial waste.

Also, studies on cytotoxicity and cell imaging showed that the cell viability of SH-SY5Y was above 90% even in the concentration of $NSCD_{200}$ at 1000 µg mL^{-1} (Fig. 7a). Under 405/488 nm laser excitation, $NSCD_{200}$ contributed the bright blue and green fluorescence in the cytoplasm region of SH-SY5Y cells (Fig. 7b), indicating that the NSCDs possessed distinctive characteristics of smaller detecting interference and non-cell damage compared with conventional CDs. Therefore, NSCDs are well suitable for biological applications, such as live-cell imaging, protein analysis, cell tracking, isolation of biomolecules etc.

In addition, $NSCD_{200}$ solution can be mixed simply with the water-soluble polymers such as polyethylene glycol (PEG-10000), polyvinyl pyrrolidone (PVP),
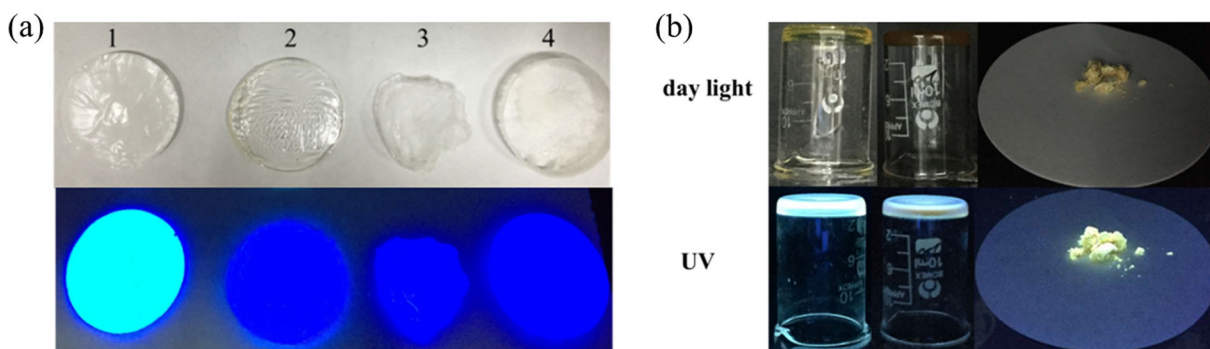

Fig. 8 Photographs of $NSCD_{200}$-polymer film samples 1–4 (1: $NSCD_{200}$-PEG10000, 2:$NSCD_{200}$-PVP, 3:$NSCD_{200}$-PAAS, 4: $NSCD_{200}$-PAM) (**a**) and solid $NSCD_{160}$, $NSCD_{200}$, $NSCD_{260}$ from left to right (**b**) under daylight (*above*) and UV light of 365 nm (*below*)

sodium polyacrylate (PAAS), and polyacrylamide (PAM) to form the fluorescent composite films. It can be seen from Fig. 8a that the composite films emitted strong blue fluorescence under UV irradiation at 365 nm even at very low concentration of $NSCD_{200}$ with $0.1 \, mg \, mL^{-1}$, demonstrating the potential of the NSCDs used in fluorescent composite materials. The PEG_{10000}/ $NSCD_{200}$ composite film exhibited the strongest fluorescence among the four samples, which could be attributed to its good dispersibility for $NSCD_{200}$ in PEG_{10000}, a well-known hydrophilic matrix. For other three samples, slight aggregation was observed most likely due to their relatively poor compatibility with water-soluble $NSCD_{200}$.

An exciting phenomenon for our as-prepared NSCDs system is that all obtained NSCDs solid samples after freeze-drying produced strong blue fluorescence for $NSCD_{160-200}$ and yellowish-green for $NSCD_{220-260}$ (Fig. 8b, taking $NSCD_{160}$, $NSCD_{200}$, $NSCD_{260}$ as representatives), which is quite different from the normal situation of CDs fluorescence quenching in the aggregation state. The apparent morphology for the dried NSCDs samples changed from viscous solid ($NSCD_{160-200}$) into fluffy powder ($NSCD_{220-260}$) mainly because of the decrease of hydrophilic groups in the samples. The blue solid fluorescence emitted from $NSCD_{160-200}$ may be attributed to the H-bond interactions generated from the surface amino/hydroxyl of the NSCDs, making the aggregated nanodots present in a dispersive state similar to that in liquid media (Xu et al. 2014; Deng et al. 2014). With the increase of the preparation temperature, the π-conjugated structure in $NSCD_{220-260}$ was enlarged by the carbonization of polyaromatic core structures with a variety of functional groups, thus leading to the solid fluorescence shifting from blue to yellowish-green (Lee et al. 2015). Interestingly, the fluorescence emission of the as-prepared bulky $NSCD_{220-260}$ showed a noticeable red shift relative to their diluted solution analogue, while most illuminated solid CDs normally show fluorescence emission at a similar position in both states of solid and solution (Xu et al. 2014). It could be ascribed to two factors, the fluorescence resonance energy transfer (FRET) and excitation dependence of $NSCD_{220-260}$. The former is mediated and caused due to that the distance of the fluorophore aligned on NSCDs is close to or less than a Förster radius under the state of aggregation,

making the excitation wavelength red shift with a small amplitude (Shi et al. 2015). The latter is predominant, in which NSCDs went through the repeated absorb-emit process under light excitation, making the re-emitted light shift to longer wavelength continuously (Wang et al. 2014a, b). It is particularly gratifying that the dried NSCDs could be repeatedly re-dispersed in aqueous solution without any aggregation, which is significant for preservation, transportation, and applications.

Conclusions

N, S co-doped carbon dots (NSCDs) with varying degrees of carbonization/aromatization and different content of multifunctional groups of $C=O$, $-NH_2$, $-OH$, $-SH$, and N, S-aromatic heterocycte were obtained from citric acid and cysteamine under different preparation temperatures. The obtained NSCDs exhibited a blue fluorescence in solution state and a tunable fluorescence in its solid state under UV light. In the latter case, with the increase in preparation temperature, fluorescence changed from strong blue to yellowish-green. The $NSCD_{200}$ showed the highest QY (81%) due to its optimal structure, and was used in complex anion detection for $Cr_2O_7^{2-}$ and $Fe(CN)_6^{3-}$, cell imaging, and preparation of fluorescent composite film, showing the satisfactory results.

References

Baker SN, Baker GA (2010) Luminescent carbon nanodots: emergent nanolights. Angew Chem Int Ed 49:6726–6744. doi:10.1002/anie.200906623

Bao L, Liu C, Zhang ZL, Pang DW et al (2015) Photoluminescence-tunable carbon nanodots: surface-state energy-gap tuning. Adv Mater 27:1663–1667. doi:10.1002/adma.201405070

Deng YH, Chen X, Wang F, Zhang XA, Zhao DX, Shen DZ (2014) Environment-dependent photon emission from solid state carbon dots and its mechanism. Nano 6:10388–10393. doi:10.1039/C4NR02544J

Ding H, Wei JS, Xiong HM (2014) Nitrogen and sulfur co-doped carbon dots with strong blue luminescence. Nano 6:13817–13823. doi:10.1039/C4NR04267K

Dong YQ, Shao JW, Chen CQ, Li H, Wang R, Chi YW et al (2012) Blue luminescent graphene quantum dots and graphene ox-ide prepared by tuning the carbonization degree of citric acid. Carbon 50:4738–4743. doi:10.1016/j.carbon.2012.06.002

Dong YQ, Pang HC, Yang HB, Guo CX, Shao JW, Chi YW et al (2013) Carbon-based dots co-doped with nitrogen and sulfur for high quantum yield and excitation-independent emission. Angew Chem Int Ed 52:7800–7804. doi:10.1002/anie.201301114

Hou J, Wang W, Zhou TY, Wang B, Li HY, Ding L (2016) Synthesis and formation mechanistic investigation of nitrogen-doped carbon dots with high quantum yields and yellowish-green fluorescence. Nano 8:11185–11193. doi:10.1039/C6NR02701F

Kasprzyk W, Bednarz S, Żmudzki P, Galica M, Bogdał D (2015) Novel efficient fluorophores synthesized from citric acid. RSC Adv 5:34795–34799. doi:10.1039/C5RA03226A

Krysmann MJ, Kelarakis A, Dallas P, Giannelis EP (2012) Formation mechanism of carbogenic nanoparticles with dual photoluminescence emission. J Am Chem Soc 134:747–750. doi:10.1021/ja204661r

Lee DW, Ma X, Jung JH, Jeong EJ, Hashemi H, Bregman A et al (2015) The effects of extended conjugation length of purely organic phosphors on their phosphorescence emission prop-erties. Phys Chem Chem Phys 17:19096–19103. doi:10.1039/C5CP01003A

Li Y, Hu Y, Zhao Y, Shi GQ, Deng LE, Hou YB et al (2011) An electrochemical avenue to green-luminescent graphene quan-tum dots as potential electron-acceptors for photovoltaics. Adv Mater 23:776–780. doi:10.1002/adma.201003819

Li HT, Kang ZH, Liu Y, Lee ST (2012) Carbon nanodots: synthe-sis, properties and applications. J Mater Chem 22:24230–24253. doi:10.1039/C2JM34690G

Liang J, Jiao Y, Jaroniec M, Qiao SZ (2012) Sulfur and nitrogen dual-doped mesoporous graphene electrocatalyst for oxygen reduction with synergistically enhanced performance. Angew Chem Int Ed 51:11496–11500. doi:10.1002/anie.201206720

Liu HP, Ye T, Mao CD (2007) Fluorescent carbon nanoparticles derived from candle soot. Angew Chem Int Ed 46:6473–6475. doi:10.1002/anie.200701271

Lu WJ, Li Y, Li RJ, Shuang SM, Dong C, Cai ZW (2016) Facile synthesis of N-doped carbon dots as a new matrix for detec-tion of hydroxy-polycyclic aromatic hydrocarbons by negative-ion matrix-assisted laser desorption/ionization time-of-flight mass spectrometry. ACS Appl Mater Interfaces 8:12976–12984. doi:10.1021/acsami.6b01510

Mirtchev P, Henderson EJ, Soheilnia N, Yip CM, Ozin GA (2012) Solution phase synthesis of carbon quantum dots as

sensitizers for nanocrystalline TiO2 solar cells. J Mater Chem 22:1265–1269. doi:10.1039/C1JM14112K

Qu D, Zheng M, Du P, Zhou Y, Zhang LG, Li D et al (2013) Highly luminescent S, N co-doped graphene quantum dots with broad visible absorption bands for visible light photocatalysts. Nano 5:12272–12277. doi:10.1039/C3NR04402E

Samantara AK, Sahu SC, Ghosh A, Jena BK (2015) Sandwiched graphene with nitrogen, sulphur co-doped CQDs: an efficient metal-free material for energy storage and conversionapplications. J Mater Chem A 3:16961–16970. doi:10.1039/C5TA03376D

Shen JH, Zhu YH, Yang XL, Li CZ (2012) Graphene quantum dots: emergent nanolights for bioimaging, sensors, catalysis and photovoltaic devices. Chem Commun 48:3686–3699. doi:10.1039/C2CC00110A

Shi JY, Chan CY, Pang YT, Ye WW, Tian F, Lyu J et al (2015) A fluorescence resonance energy transfer (FRET) biosensor based on graphene quantum dots (GQDs) and gold nanopar-ticles (AuNPs) for the detection of mecA gene sequence of *Staphylococcus aureus*. Biosens Bioelectron 67:595–600. doi:10.1016/j.bios.2014.09.059

Song ZQ, Quan FY, Xu YH, Liu ML, Cui L, Liu JQ (2016) Multifunctional N, S co-doped carbon quantum dots with pH- and thermo-dependent switchable fluorescent properties and highly selective detection of glutathione. Carbon 104:169–178. doi:10.1016/j.carbon.2016.04.003

Wang BB, Cheng QJ, Wang LH, Zheng K, Ostrikov K (2012) The effect of temperature on the mechanism of photoluminescence from plasma-nucleated, nitrogenated car-bon nanotips. Carbon 50:3561–3571. doi:10.1016/j.carbon.2012.03.028

Wang Y, Kalytchuk S, Zhang Y, Shi HC, Kershaw SV, Rogach AL (2014a) Thickness-dependent full-color emission tunability in a flexible carbon dot ionogel. J Phys Chem Lett 5:1412–1420. doi:10.1021/jz5005335

Wang WP, Lu YC, Huang H, Wang AJ, Chen JR, Feng JJ (2014b) Solvent-free synthesis of sulfur- and nitrogen-co-doped fluo-rescent carbon nanoparticles from glutathione for highly selective and sensitive detection of mercury (II) ions. Sensors Actuators B Chem 202:741–747. doi:10.1016/j.snb.2014.06.010

Wu P, Li Y, Yan XP (2009) CdTe quantum dots (QDs) based kinetic discrimination of Fe^{2+} and Fe^{3+}, and CdTe QDs-fenton hybrid system for sensitive photoluminescent detec-tion of Fe^{2+}. Anal Chem 81:6252–6257. doi:10.1021/ac900788w

Xu MH, He GL, Li ZH, He FJ, Gao F, Su YJ et al (2014) A green heterogeneous synthesis of N-doped carbon dots and their photoluminescence applications in solid and aqueous states. Nano 6:10307–10315. doi:10.1039/C4NR02792B

Xu Q, Pu P, Zhao JG, Dong CB, Gao C, Chen YS et al (2015a) Preparation of highly photoluminescent sulfur-doped carbon dots for Fe (III) detection. J Mater Chem A 3:542–546. doi:10.1039/C4TA05483K

Xu MH, Xu SS, Yang Z, Shu MJ, He GL, Huang D et al (2015b) Hydrophilic and blue fluorescent N-doped carbon dots from tartaric acid and various alkylol amines under microwave irradiation. Nano 7:15915–15923. doi:10.1039/C5NR04209G

Xue MY, Zhang LL, Zou MB, Lan CQ, Zhan ZH, Zhao SL (2015) Nitrogen and sulfur co-doped carbon dots: a facile and green

fluorescence probe for free chlorine. Sensors Actuators B Chem 219:50–56. doi:10.1016/j.snb.2015.05.021

Yang ZC, Li X, Wang J (2011) Intrinsically fluorescent nitrogen-containing carbon nanoparticles synthesized by a hydrothermal process. Carbon 49:5207–5212. doi:10.1016/j.carbon.2011.07.038

Yang Z, Yao Z, Li GF, Fang GY, Nie HG, Liu Z et al (2012) Sulfur-doped graphene as an efficient metal-free cathode catalyst for oxygen reduction. ACS Nano 6:205–211. doi:10.1021/nn203393d

Zhang WX, Dai DJ, Chen XF, Guo XX, Fan JY et al (2014) Red shift in the photoluminescence of colloidal carbon quantum dots induced by photon reabsorption. Appl Phys Lett 104:091902. doi:10.1063/1.4867487

Zhao AD, Zhao CQ, Li M, Ren JS, Qu XG (2014) Ionic liquids as precursors for highly luminescent, surface-different nitrogen-doped carbon dots used for label-free detection of Cu^{2+}/Fe^{3+} and cell imaging. Anal Chim Acta 809:128–133. doi:10.1016/j.aca.2013.10.046

Zheng M, Xie ZG, Qu D, Li D, Du P, Jing XB et al (2013) On−off−on fluorescent carbon dot nanosensor for recognition of chromium (VI) and ascorbic acid based on the inner filter effect. ACS Appl Mater Interfaces 5:13242–13247. doi:10.1021/am4042355

Zhou J, Wang C, Qian ZS, Chen CC, Ma JJ, Du GH et al (2012) Highly efficient fluorescent multi-walled carbon nanotubes functionalized with diamines and amides. J Mater Chem 22:11912–11914. doi:10.1039/C2JM31192E

Zhou J, Yang Y, Zhang CY (2013) A low-temperature solid-phase method to synthesize highly fluorescent carbon nitride dots with tunable emission. Chem Commun 49:8605–8607. doi:10.1039/C3CC42266F

Zhu SJ, Meng QN, Wang L, Zhang JH, Song YB, Jin H et al (2013) Highly photoluminescent carbon dots for multicolor patterning, sensors, and bioimaging. Angew Chem Int Ed 52:3953–3957. doi:10.1002/anie.201300519